JOURNAL OF Materials CHEMISTRY

Crystal structure, thermal and magnetic properties of $La_3Co_3O_8$. Phase relations for $LaCoO_{3-\delta}$ ($0.00 \leqslant \delta \leqslant 0.50$) at 673 K

Ole H. Hansteen,[a] Helmer Fjellvåg*[a] and Bjørn C. Hauback[b]

[a] *Department of Chemistry, University of Oslo, N-0315 Oslo, Norway*
[b] *Institutt for energiteknikk, N-2007 Kjeller, Norway*

Phase relations including reoxidation and decomposition reactions were investigated for samples with nominal composition $LaCoO_{3-\delta}$ ($0.00 \leqslant \delta \leqslant 0.50$). $LaCoO_{3-\delta}$ was synthesized by isothermal reduction at 673 K. For $\delta = 0.50$ and 0.33 distinct phases occur, namely $La_2Co_2O_5$ and $La_3Co_3O_8$. $La_2Co_2O_5$ oxidizes *via* $La_3Co_3O_8$ to $LaCoO_3$. None of these reduced, vacancy ordered phases show indications for any larger non-stoichiometry. $La_2Co_2O_5$ and $La_3Co_3O_8$ are metastable, and undergo irreversible decomposition reactions to CoO and the Ruddlesden–Popper type phases $La_{m+1}Co_mO_{3m+1}$, $m = 1$ and 3, upon heating under inert atmosphere. The crystal structure of $La_3Co_3O_8$ is determined on the basis of simultaneous refinement of high-resolution powder X-ray diffraction and neutron diffraction data. The space group is $P2_1$, $a = 555.93$ pm, $b = 541.51$ pm, $c = 1177.3$ pm, $\beta = 90.144^\circ$ at RT; $R_{wp}(PXD) = 4.6\%$, $R_{wp}(PND) = 6.1\%$, $R_p(PXD) = 3.6\%$, $R_p(PND) = 4.7\%$. $La_3Co_3O_8$ adopts a structure which is an intermediate between the brownmillerite and the perovskite type structures. Double layers of corner-sharing CoO_6 octahedra are connected by layers with chains of corner-sharing CoO_4 tetrahedra running along [010]. $La_3Co_3O_8$ orders antiferromagnetically at temperatures below $T_N = 35$ K. A probable magnetic structure is described on the basis of powder neutron diffraction data. The magnetic moments are $\mu_{Co(1),\ tet} = 3.5 \pm 0.1\ \mu_B$, $\mu_{Co(2),\ oct} = 1.7 \pm 0.2\ \mu_B$ and $\mu_{Co(3),\ oct} = 2.0 \pm 0.2\ \mu_B$.

Introduction

Considerable attention has been devoted to the stability and properties of perovskite type materials upon reduction, partly because of their possible use under reducing conditions in catalysts, sensors and fuel cells. Quite typically, the partially reduced intermediate phases are structurally closely related to the perovskite type structure. In the La–Co–O system two different series of intermediate phases can be obtained upon reduction of $LaCoO_3$. Reduction at high temperatures, $T > 900$ K, leads to intermediate phases of the Ruddlesden–Popper type, $La_{m+1}Co_mO_{3m+1}$, before complete reduction to Co and La_2O_3 finally occurs.[1] However, for $T < 900$ K intermediate phases of the series $La_nCo_nO_{3n-1}$ result.[2] $La_2Co_2O_5$ ($n = 2$) is the only phase of the $La_nCo_nO_{3n-1}$ series for which crystal structure data (brownmillerite type) have been reported,[2,3] but clear indications for an intermediate phase in the composition range $0.00 \leqslant \delta \leqslant 0.50$ was shown by Tilset *et al.*[4] using temperature programmed reduction (TPR). $A_nM_nO_{3n-1}$ phases with $n = 2$, 3, 4 and 5 have been described in other perovskite systems,[5–8] where A typically denotes an alkali, alkaline-earth or rare-earth element and M is a 3*d* or 4*d* transition element. For all the $A_nM_nO_{3n-1}$ phases the crystal structures retain the perovskite type arrangement of the cations, whereas the oxygen deficiency results in oxygen vacancy ordering and the formation of large supercells. The type of superstructure varies and depends strongly on the identity of the M-cation.

The present study focuses on the phase relations for $LaCoO_{3-\delta}$, $0.00 \leqslant \delta \leqslant 0.50$, at 673 K. The crystal and magnetic structures of the intermediate phase $La_3Co_3O_8$ ($n = 2$, $\delta = 0.33$) have been determined with basis in a combined analysis of high resolution powder X-ray diffraction data collected at ESRF and powder neutron diffraction data.

Experimental

Synthesis

$LaCoO_{3-\delta}$ was prepared by isothermal reduction of single phase $LaCoO_3$. The $LaCoO_3$ was first prepared by a citrate precursor method.[9] The starting materials for the synthesis of $LaCoO_3$ were La_2O_3 (99.99% Molycorp), $Co(CH_3COO)_2{\cdot}4H_2O$ (>99% Fluka) and citric acid monohydrate, $C_3H_4(OH)(CO_2H)_3{\cdot}H_2O$ (>99.8% Riedel-de Haën). Single phase $LaCoO_3$ was obtained after calcination of the precursor powder in air at 1300 K for 110 h with two intermediate grindings followed by repelletization. Phase purity was assured from powder X-ray diffraction. The isothermal reduction of $LaCoO_3$ to $LaCoO_{3-\delta}$ (nominally) was performed in sealed silica glass ampoules using chips of Zr (99.5% A. D. Mackay Inc.) as reducing agent (oxygen getter). The ampoules, with the samples, were repeatedly flushed with argon before evacuation and sealing in order to minimize the amount of gaseous oxygen in the system prior to the reduction. The sample was held in an alumina crucible at 673 K, and was separated (by approximately 160 mm) from the Zr, which was positioned in the warmer zone of the furnace at 873 K in order to assure complete oxidation to ZrO_2. The total reaction

$$2\ LaCoO_3 + \delta Zr \rightarrow 2\ LaCoO_{3-\delta} + \delta ZrO_2 \qquad (1)$$

is favoured due to the high thermodynamic stability of ZrO_2 at the prevailing conditions. After reaction and equilibration for seven days, all samples were cooled in ice-water. The ampoules were opened in an argon filled glovebox [$p(O_2)$ and $p(H_2O) < 1$ ppm]. Care was taken to assure inert atmosphere during storage, handling and subsequent characterisation of specimens. Preliminary studies showed that $LaCoO_{3-\delta}$ reoxidizes rapidly (and reversibly) when subjected to air at ambient temperature and pressure. This emphasizes the importance of inert handling of the reduced samples.

Powder diffraction

Room temperature powder X-ray diffraction (PXD) data were collected for all samples with a Guinier-Hägg camera using Si as internal standard ($a = 543.1065$ pm). The sample holders were filled with oil and sealed with Scotch tape on top and bottom. The sample adhered to the bottom tape which prevented it from dispersing into the oil. Both $CrK\alpha_1$ (detection limit for impurities *ca.* 0.3 wt.%)[10] and $CuK\alpha_1$ radiation were used. The programs TREOR[11] and UNITCELL[12] were used

for unit cell indexing and least squares determination of unit cell dimensions. Synchrotron (SR) PXD data were collected for $La_3Co_3O_8$ with the powder diffractometer in Debye-Scherrer mode at the Swiss Norwegian Beam Line (BM1) at ESRF (Grenoble). Monochromatic X-rays of wavelength 110.094 pm were obtained from a channel-cut Si(111) crystal. The sample was contained in a sealed and rotating glass capillary, diameter 0.5 mm. Intensity data were collected at 298 K between $2\theta = 5$ and 61.5° in steps of $\Delta(2\theta) = 0.007°$. Powder neutron diffraction (PND) data were collected for $La_3Co_3O_8$ with the two-axis powder diffractometer PUS at the JEEP II reactor, Kjeller (Norway). A cylindrical sample holder of vanadium, carefully sealed with an indium washer, was used. Monochromatised neutrons of wavelength 153.79 pm were obtained by reflection from Ge(511) of the focusing composite germanium monochromator. The scattered intensities were measured by two detector units. Each detector unit contains a vertical stack of seven position sensitive ^{3}He detectors which covers 20° in 2θ. Intensity data were collected at 10 and 298 K between $2\theta = 10°$ and 130° in steps of $\Delta(2\theta) = 0.05°$. The GSAS program package[13] was used for the combined Rietveld-type profile refinements of powder synchrotron X-ray and neutron diffraction data collected at 298 K. Table 1 summarises characteristic features of the data sets and the variable parameters entering the least-squares refinements. The background was modelled by cosine Fourier series polynomials for both datasets. The peak shape of the synchrotron diffraction pattern was modelled by a pseudo-Voigt function using three Gaussian halfwidth parameters (U, V, W) and two Lorentzian coefficients (one Scherrer broadening coefficient and one strain broadening coefficient). For the PND data, the peak shape was modelled by a Gaussian function. The scattering lengths $b_{La} = 8.27$ fm, $b_{Co} = 2.53$ fm and $b_O = 5.81$ fm were taken from the GSAS library. For profile refinement of the PND data collected at 10 K (crystal and magnetic structure) the Hewat version[14] of the Rietveld program[15] was used.

High temperature PXD data were collected upon continuous heating using a Guinier-Simon camera (Enraf Nonius) and Cu$K\alpha_1$ radiation. The sample was kept in a rotating silica glass capillary. Photographic film was used as detector and the temperature change was synchronised with the movement of the film cassette. The temperature was calibrated by means of measurement of the thermal expansion of silver.[16]

Thermal analysis

Thermogravimetric (TGA) and differential thermal (DTA) analyses were performed with a Perkin Elmer TGA7 and DTA7. Data reduction was performed with standard programs for the systems.

Table 1 Characteristic features of the powder synchrotron X-ray (298 K) and neutron diffraction (10, 298 K) data sets for $La_3Co_3O_8$, and list of parameters entering the profile refinements

	PXD(SR)			PND	
measured data points	8052			2499	
reflections (hkl)	349			694	
λ/pm	110.094			153.79	
scale factor	1			1	
zero point	1			1	
profile parameters	5			3	
unit cell dimensions			4[a]		
positional parameters			30[a]		
isotropic displacement factors			3[a]		
magnetic components				(6)[b]	
background coefficients	16			9	
refinable parameters	23	+	37 +	14	= 74

[a]Common parameters for PXD(SR) and PND in the combined refinements. [b]Only refined for the 10 K data.

Magnetic measurements

Magnetic susceptibility data were measured by a Quantum Design SQUID-magnetometer (MPMS) in the temperature range 2–300 K for magnetic fields (H) up to 50.0 kOe. All samples were zero field cooled and the temperature dependence of the magnetic susceptibility was measured on heating. The samples were held in evacuated and sealed spherical silica glass ampoules. The measured magnetic susceptibility was corrected for diamagnetic contributions from the sample container and from core electrons.

Results and Discussion

Phase relations for $LaCoO_{3-\delta}$ ($0.00 \leqslant \delta \leqslant 0.50$); reoxidation and decomposition

Ten samples of $LaCoO_{3-\delta}$ with different nominal oxygen contents, $0.00 \leqslant \delta \leqslant 0.50$, were synthesized. These included $\delta = 0.25$, 0.33 and 0.50, which respectively correspond to the $n = 4$, 3 and 2 phases of the suggested homologous series $La_nCo_nO_{3n-1}$. Analysis of the PXD patterns at 298 K shows that three distinct phases exist, namely $LaCoO_3$ ($\delta = 0.00$, $n = \infty$), $La_3Co_3O_8$ ($\delta = 0.33$, $n = 3$) and $La_2Co_2O_5$ ($\delta = 0.50$, $n = 2$). All other samples, including those with only minor deviation from the stoichiometric compositions $n = 2$, 3 and ∞, were identified to consist of two-phase mixtures of the above phases and indicated no significant non-stoichiometry for these phases under the presently used synthesis conditions. The general formula $LaCoO_{3-\delta}$ therefore represent a two-phase mixture of $LaCoO_3$ and $La_3Co_3O_8$ for $0.00 < \delta < 0.33$ and a two-phase mixture of $La_2Co_2O_5$ and $La_3Co_3O_8$ for $0.33 < \delta < 0.5$.

Two successive phase reactions were verified by means of high temperature PXD on oxidation of $La_2Co_2O_5$ in air, first to $La_3Co_3O_8$ (around 310 K) and then to $LaCoO_3$ (around 360 K). Fig. 1 shows, schematically, the changes in the high temperature PXD pattern of $La_2Co_2O_5$ upon oxidation. The sample was subjected to air immediately before starting the experiment. The single phase regimes for $La_nCo_nO_{3n-1}$ with $n = 2$, 3 and ∞, respectively, are separated by two-phase regions (shaded background). TGA and DTA shows a stepwise oxidation of $La_2Co_2O_5$, Fig. 2. The first step with onset at 360 K corresponds approximately to the composition of $La_3Co_3O_8$. Similar stepwise oxidation occurs for all compositions in the range $0.33 < \delta \leqslant 0.50$, whereas for compositions in the range $0.00 \leqslant \delta \leqslant 0.33$ the oxidation proceeds through a single step with onset at 425 K as shown for $La_3Co_3O_8$ in Fig. 2. PXD of the oxidized samples verifies a complete oxidation to $LaCoO_3$. The composition of $LaCoO_3$ in air is very close to stoichiometric at the temperatures used for the oxidations,[17] thus the measured weight increment was used to verify the oxygen

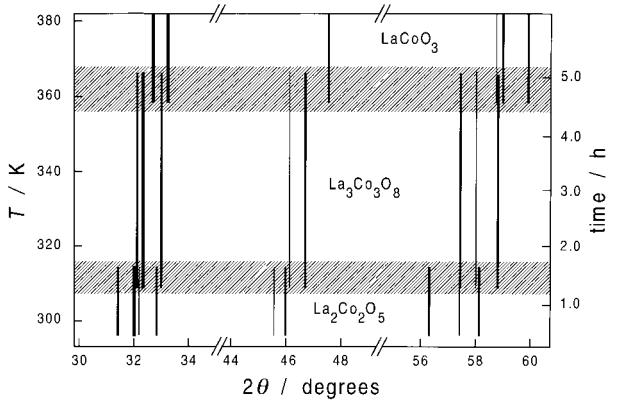

Fig. 1 Schematic presentation of the high temperature PXD pattern during oxidation of $La_2Co_2O_5$ in air. Heating rate 0.23 K min^{-1}, $\lambda = 154.06$ pm.

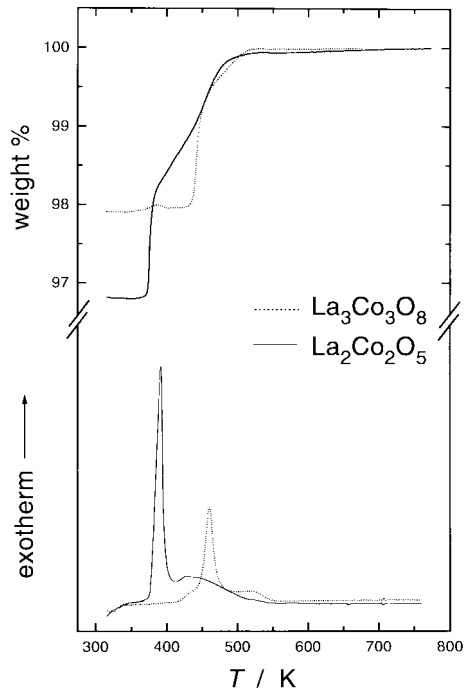

Fig. 2 Thermogravimetric and differential thermal analysis data for oxidation of $La_2Co_2O_5$ and $La_3Co_3O_8$ in air. Heating rate 5 K min^{-1}.

content of the reduced samples. The accuracy of the oxygen content (δ) is estimated to be ± 0.01.

The initial rapid oxidation of the reduced $LaCoO_{3-\delta}$ samples at low temperatures, see Fig. 2, shows that the reduced phases are thermodynamically unstable relative to $LaCoO_3$ at ambient. The relatively open crystal structures of the vacancy ordered, reduced phases facilitate easy oxygen transport into the samples, see below for a detailed description of the crystal structure of $La_3Co_3O_8$. Many brownmillerite related oxides are also known to be good oxide ion conductors.[18] The TGA data show that the oxidation rate is reduced when complete oxidation is approached, giving rise to a shoulder on the DTA peak. Sample specific parameters like particle size and size distribution and possibly also the formation of a (dense) surface layer of $LaCoO_3$, not detectable with high temperature PXD, may effect the rate of oxidation. From the schematic presentation of the crystal structures of $La_2Co_2O_5$, $La_3Co_3O_8$ and $LaCoO_3$ in Fig. 3, showing the octahedral and tetrahedral coordination polyhedra for cobalt, it is clear that the oxidation from $La_2Co_2O_5$ to $La_3Co_3O_8$ does not only involve filling some of the vacancies with oxygen atoms. A substantial, three dimensional reorganisation of the oxygen sublattice is required (some routes are indicated by arrows in Fig. 3). It is remarkable that oxidation is activated at room temperature. However, the substantial oxidation enthalpy evolved, even to be felt by touching a crucible with $La_2Co_2O_5$, implies high local temperature in the material and the oxygen diffusion probably takes place at a local temperature far higher than indicated in Fig. 2. The poorly defined second step of the oxidation of $La_2Co_2O_5$ can similarly be explained by local temperatures sufficiently high to simultaneously activate oxidation of the intermediate phase $La_3Co_3O_8$.

DTA curves for $La_2Co_2O_5$ and $La_3Co_3O_8$, obtained on heating the samples in evacuated and sealed ampoules, are shown in Fig. 4. The phases undergo irreversible decomposition reactions into Ruddlesden–Popper (RP) type phases $La_{m+1}Co_mO_{3m+1}$, $m=1$ and 3, and CoO according to eqn. (2) and (3).

$$La_2Co_2O_5 \rightarrow La_2CoO_4 + CoO \quad (2)$$

$$2\ La_3Co_3O_8 \rightarrow La_4Co_3O_{10} + La_2CoO_4 + 2\ CoO \quad (3)$$

The reaction products were confirmed by PXD on samples heated to 1275 K. The average oxidation state of cobalt is preserved during these decompositions. The decomposition is furthermore manifested in the temperature dependence of the magnetic susceptibility of $La_2Co_2O_5$.[3] The decomposition of $La_2Co_2O_5$ with onset at 940 K is a single step, exothermic reaction, see Fig. 4. Both reactants and products contain solely divalent cobalt. The decomposition of $La_3Co_3O_8$ (onset at 910–950 K) is complex and spans a much broader temperature range involving an initial endothermal step followed by two exothermal steps. The average oxidation state for cobalt in $La_3Co_3O_8$ corresponds to a ratio $Co^{II}/Co^{III}=2$. No other phases are known in the La–Co–O system with this Co^{II}/Co^{III} ratio. The complex decomposition reaction of $La_3Co_3O_8$ to the final products ends with localisation of all trivalent cobalt atoms into one of the product phases, $La_4Co_3O_{10}$ ($Co^{II}/Co^{III}=0.5$). In order to identify intermediate products during decomposition, a second sample was similarly heated in evacuated and sealed ampoules to 960 K within the DTA apparatus. PXD at 298 K showed the presence of (non-decomposed) $La_3Co_3O_8$, $La_2CoO_{4+\delta}$ ($Co^{II}/Co^{III}=(1-2\delta)/2\delta$), $La_2Co^{II}{}_2O_5$ and $Co^{II}O$. However, a few additional PXD reflections were visible, and may possibly stem from either the unstable RP-phase $La_3Co_2O_7$ [$m=2$, $Co^{II}/Co^{III}=1$, not yet described] or $La_4Co_4O_{11}$ ($n=4$, $Co^{II}/Co^{III}=1$, not yet described). There are no indications for any (major) release of oxygen. $La_4Co_3O_{10}$ was not detected at this intermediate stage of the decomposition reaction. Hence, in order to retain the average oxidation state of cobalt during decomposition, one of these two possible intermediate phases might temporarily exist. The formation

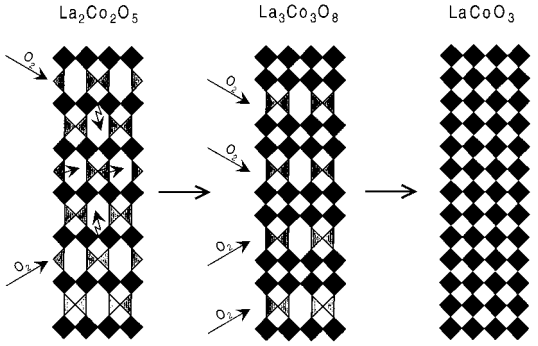

Fig. 3 Schematic presentation of the crystal structures of $La_2Co_2O_5$, $La_3Co_3O_8$ and $LaCoO_3$, projected on the plane normal to the chains of tetrahedra. Diamonds represent CoO_6 octahedra, triangles represent CoO_4 tetrahedra; La atoms are omitted for clarity. The arrows (left) indicate the required reorganisation of the oxygen sublattice upon oxidation from $La_2Co_2O_5$ to $La_3Co_3O_8$.

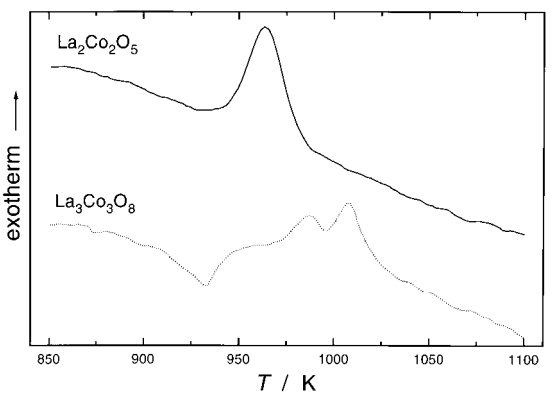

Fig. 4 Differential thermal analysis data for $La_2Co_2O_5$ (——) and $La_3Co_3O_8$ (····) in sealed, evacuated ampoules. Heating rate 10 K min^{-1}.

and subsequent decomposition of an intermediate phase is consistent with the stepwise decomposition indicated by DTA. The irreversible exothermic decompositions of the $La_nCo_nO_{3n-1}$ phases suggest that the reduced, vacancy ordered perovskite-type phases are thermodynamically metastable. The formation of the $La_nCo_nO_{3n-1}$ phases by low temperature reduction is possible owing to non-sufficient energy for diffusion of cations, which would be required for the formation of the (stable) RP-type phases $La_{m+1}Co_mO_{3m+1}$. It is possible that the temperature of the decomposition reaction may indicate the onset of cation diffusion in these materials. The fact that the $La_nCo_nO_{3n-1}$ compounds are unstable at temperatures where cation diffusion is facilitated prevents their direct synthesis from single component starting materials.

Crystal structure of $La_3Co_3O_8$

All reflections for $La_3Co_3O_8$ in the Guinier-Hägg PXD pattern at 298 K could satisfactorily be indexed using a primitive orthorhombic unit cell (*Pbmm*; non-standard setting of space group *Pmma*): $a=555.9(1)$ pm, $b=541.55(8)$ pm, $c=1177.9(2)$ pm, with relations to the ideal cubic perovskite unit cell, $\bar{a}=\bar{a}_c-\bar{b}_c$, $\bar{b}=\bar{a}_c+\bar{b}_c$, and $\bar{c}=3\bar{c}_c$. Based on the chemical composition and the relationship to the cubic perovskite unit cell, the initial structural model for $La_3Co_3O_8$ was assumed to contain double perovskite type layers of octahedrally coordinated cobalt connected by layers with chains of corner-sharing CoO_4 tetrahdra (as found in the brownmillerite type structure for $La_2Co_2O_5$).[3] This $A_3M_3O_8$ type structure was first reported by Grenier *et al.*[7] Support for this model was obtained from comparison of observed intensities and pattern calculations with the LAZY-PULVERIX program[19] using atomic coordinates for $Ca_3Mn_{1.35}Fe_{1.65}O_{8.02}$ (space group *Pmma*).[20]

Careful inspection of the synchrotron PXD intensity profiles showed a small, systematic splitting of the orthorhombic reflections of the types (*hkl*) and (*h*0*l*). This indicates that the real symmetry is monoclinic ($\beta\neq90^\circ$), see Table 2. Examples of the peak splitting are given in Fig. 5. This shows that high resolution synchrotron X-ray data are essential in order to determine the correct symmetry of the crystal structure. However, for X-ray diffraction experiments on compounds in the La–Co–O system, the major scattering contributions come from the heavy La and Co atoms. Hence, powder neutron diffraction data are required for proper determination of small oxygen displacements (*e.g.* tilting or distortion of the coordination polyhedra). These are hardly detectable with X-rays.

The only systematic absent reflections (0*k*0) for $k=2n+1$ in

Table 2 Unit cell data for $La_3Co_3O_8$ and *R*-values. Calculated standard deviations in parentheses

		298 K	10 K
space group		$P2_1$	$P2_1$
a/pm		555.934(1)	555.0(1)
b/pm		541.514(3)	539.56(3)
c/pm		1177.27(1)	1174.0(2)
β/°		90.144(1)	90.144[b]
$V/10^8$pm^3		3.54412(4)	3.5153(3)
Z		2	2
R_p (%)[a]	PXD(SR)	3.6	
	PND	4.7	8.5[c]
R_{wp} (%)[a]	PXD(SR)	4.6	
	PND	6.1	14.3
R_{exp} (%)[a]	PXD(SR)	3.0	
	PND	4.0	7.3
χ^2		2.28	3.88

[a] $R_p=100(\Sigma|I_o-I_c|/\Sigma I_o)$, $R_{wp}=100(\Sigma w(I_o-I_c)^2/\Sigma wI_o^2)^{-1/2}$, $R_{exp}=R_{wp}/\sqrt{\chi^2}$ according to ref. 13 (298 K) and ref. 14 and 15 (10 K). [b] Not refined because the resolution of the PND data is too low to resolve the splitting of the peaks. [c] Combined refinement, crystallographic ($R_N=7.3\%$) and magnetic ($R_M=19.1\%$).

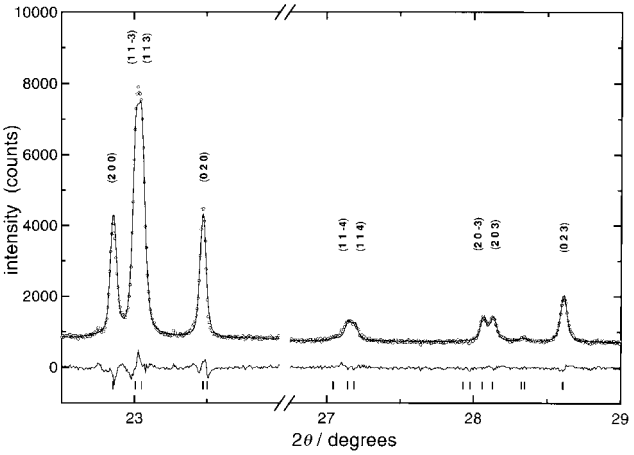

Fig. 5 Selected parts of the synchrotron PXD profile for $La_3Co_3O_8$ showing monoclinic splitting of certain reflections. Miller indices are given (space group $P2_1$). Experimental points marked by open circles, full line marks calculated profile, lower full line marks difference plot. Positions for Bragg reflections are marked by vertical bars. Wavelength $\lambda=110.094$ pm.

the diffraction patterns (Fig. 6) indicate either of two possible space groups, $P2_1/m$ or $P2_1$. For space group $P2_1/m$ with all atoms in fully occupied positions, *i.e.* with the oxygen atom O(1) (Fig. 7) in position 2a (0,0,0), strongly distorted CoO_4 tetrahedra result. The subsequent Rietveld profile refinement of the combined synchrotron PXD and PND data for such a model gave a poor *R*-value for the PND data, $R_{wp}(PND)=12.1\%$. For the X-ray data the refinement was satisfactory, $R_{wp}(PXD)=4.7\%$. However, when the two O(1) atoms were randomly distributed over the general position 4f (*x*,*y*,*z*), the refinement converged satisfactorily giving $R_{wp}(PND)=6.3\%$ and $R_{wp}(PXD)=4.7\%$ [atomic coordinates (0.148, 0.839, 0.003) for O(1)]. On the other hand, for space group $P2_1$ all atoms can be placed in fully occupied positions, with O(1) in two equivalent positions as shown in Fig. 7. The *y*-coordinate for at least one atom has to be fixed in order to fix the origin for space group $P2_1$. However, there was no significant difference between the *R*-values for refinements with only one *y*-coordinate fixed and refinements where all *y*-coordinates [except for Co(1) and O(1)] were fixed. The number of free variables could thereby be reduced. Actually, fixing all *y*-coordinates [except for Co(1) and O(1)] reduced the distortion of the coordination polyhedra of cobalt, and the results of this refinement are given in Tables 2–4 and Fig. 6 and 7. Introduction of soft constraints on Co—O and O—O interatomic distances did not reduce the distortions of the coordination polyhedra for any of the proposed models using the present powder diffraction data. The fractional atomic coordinates as well as the isotropic displacement factors were approximately equal for refinements according to the structural descriptions based on $P2_1/m$ and $P2_1$. Thus, the major difference between the two models is whether the O(1) oxygen atom is randomly distributed over four (half-filled) equivalent positions ($P2_1/m$) or located on two equivalent positions ($P2_1$).

The crystal structure for $La_3Co_3O_8$ is shown in Fig. 7. It consists of double perovskite type layers of corner-sharing CoO_6 octahedra [Co(2) and Co(3)] parallel to the *ab*-plane of the unit cell, connected by layers containing chains of corner-sharing CoO_4 tetrahedra. The chains of tetrahedra run parallel to [010]. In order to approach regular tetrahedral coordination for Co(1), the oxygen atoms and Co(1) are somewhat displaced relative to the perovskite atomic arrangement. This is analogous to the displacements described for the related phase $La_2Co_2O_5$.[3] Despite the atomic displacements there are still considerable distortions of the tetrahedra especially along [001] as shown by the large O(2)—Co(1)—O(3)

Table 3 Fractional atomic coordinates for $La_3Co_3O_8$ at 298 K. Calculated standard deviations in parentheses. Space group $P2_1$, all atoms in general site 2a(x,y,z). Isotropic displacement factors ($B_{iso}/10^4pm^2$): $B_{iso}(La)=1.06(3)$, $B_{iso}(Co)=0.0(1)$, $B_{iso}(O)=0.77(4)$.

atom	x	y^a	z
La(1)	0.7397(7)	0.25	0.8101(4)
La(2)	0.7319(7)	0.25	0.1894(4)
La(3)	0.7540(7)	0.25	0.4961(5)
Co(1)	0.199(1)	0.208(1)	0.001(1)
Co(2)	0.237(2)	0.25	0.336(1)
Co(3)	0.248(2)	0.25	0.6692(9)
O(1)	0.144(1)	0.835(1)	0.000(2)
O(2)	0.294(2)	0.25	0.1572(7)
O(3)	0.310(2)	0.25	0.8500(8)
O(4)	0.494(3)	0.00	0.3498(3)
O(5)	0.489(3)	0.50	0.3498(3)
O(6)	0.188(1)	0.25	0.4888(7)
O(7)	0.002(3)	0.00	0.3158(3)
O(8)	0.005(3)	0.50	0.3158(3)

[a]All y-coordinates are fixed and not refined except for Co(1) and O(1), see text.

angle and short Co(1)—O(2) and Co(1)—O(3) interatomic distances (Table 4). Calculated bond valences for the Co-atoms according to Brown and Altermatt[21] {using $v_i=\Sigma\exp[(D_i-d_i)/0.37]$, $D_i=1.695$, $d_i=$experimentally determined interatomic Co—O distances} are $v_{Co(1)}=1.92$, $v_{Co(2)}=3.16$ and $v_{Co(3)}=2.44$. This indicates that divalent cobalt of $La_3Co^{II}{}_2Co^{III}O_8$ occupies the tetrahedral site, and furthermore that a charge ordering may occur for the octahedral sites with Co^{III} for Co(2) and Co^{II} for Co(3).

Magnetic properties of $La_3Co_3O_8$

Magnetic susceptibility (χ_m) data for $La_3Co_3O_8$ are shown in Fig. 8. At low temperatures, long range antiferromagnetic ordering is indicated below $T_N=35$ K. The magnetic suscepti-

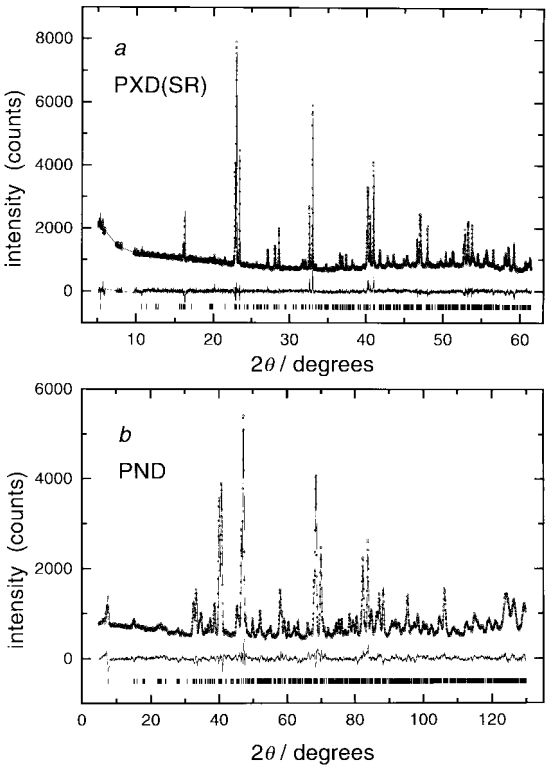

Fig. 6 (*a*) Synchrotron PXD ($\lambda=110.094$ pm) and (*b*) PND ($\lambda=153.79$ pm) profiles for $La_3Co_3O_8$ at 298 K. Experimental points marked by open circles, full line marks calculated profile, lower full line marks difference plot. Positions for Bragg reflections are marked by vertical bars.

Table 4 Selected interatomic distances (pm) and bond angles (°) for $La_3Co_3O_8$ at 298 K; calculated standard deviations in parentheses, atom numbers refer to Fig. 7

tetrahedron:	Co(1)—$O(1)_1$	204(1)	$O(1)_1$—Co(1)—$O(1)_2$ 101.3(3)
	Co(1)—$O(1)_2$	203(1)	$O(1)_1$—Co(1)—O(2) 99.4(7)
	Co(1)—O(2)	192(1)	$O(1)_2$—Co(1)—O(2) 103.1(8)
	Co(1)—O(3)	190(1)	$O(1)_1$—Co(1)—O(3) 99.2(7)
			$O(1)_2$—Co(1)—O(3) 105.1(8)
			O(2)—Co(1)—O(3) 142.2(4)
octahedra:	Co(2)—O(2)	213(2)	O(2)—Co(2)—O(4,5,7,8) 88.4–89.0(5)
	Co(2)—O(4)	197(1)	O(6)—Co(2)—O(4,5,7,8) 91.2–91.5(5)
	Co(2)—O(5)	196(1)	O(4)—Co(2)—O(5) 87.1(6)
	Co(2)—O(6)	182(1)	O(4)—Co(2)—O(7) 91.0 (4)
	Co(2)—O(7)	189(1)	O(5)—Co(2)—O(8) 90.2(6)
	Co(2)—O(8)	189(1)	O(7)—Co(2)—O(8) 91.5(6)
			O(2)—Co(2)—O(6) 179.8(2)
			O(4)—Co(2)—O(8) 176.2(7)
			O(5)—Co(2)—O(7) 176.9(7)
	Co(3)—O(3)	216(1)	O(3)—Co(3)—O(4,5,7,8) 89.7–91.4(5)
	Co(3)—O(4)	199(1)	O(6)—Co(3)—O(4,5,7,8) 88.8–90.1(5)
	Co(3)—O(5)	201(1)	O(4)—Co(3)—O(5) 85.4(6)
	Co(3)—O(6)	215(1)	O(4)—Co(3)—O(7) 93.0(4)
	Co(3)—O(7)	195(1)	O(5)—Co(3)—O(8) 87.7(6)
	Co(3)—O(8)	196(1)	O(7)—Co(3)—O(8) 93.8(4)
			O(3)—Co(3)—O(6) 179.7(2)
			O(4)—Co(3)—O(8) 178.6(6)
			O(5)—Co(3)—O(7) 178.1(6)
	La(1)—O	237–274, 320(1)	8+1
	La(2)—O	238–276, 315(1)	8+1
	La(3)—O	242–293, 315(1)	11+1
polyhedra tilt angles/°	Co(1)—O(1)—Co(1)	118.4(7)	
	Co(1)—O(2)—Co(2)	154.3(7)	
	Co(1)—O(3)—Co(3)	150.9(7)	
	Co(2)—O(6)—Co(3)	162.5(7)	
	Co(2)—O(4,5)—Co(3)	168.8(7)	
	Co(2)—O(7,8)—Co(3)	167.5(7)	

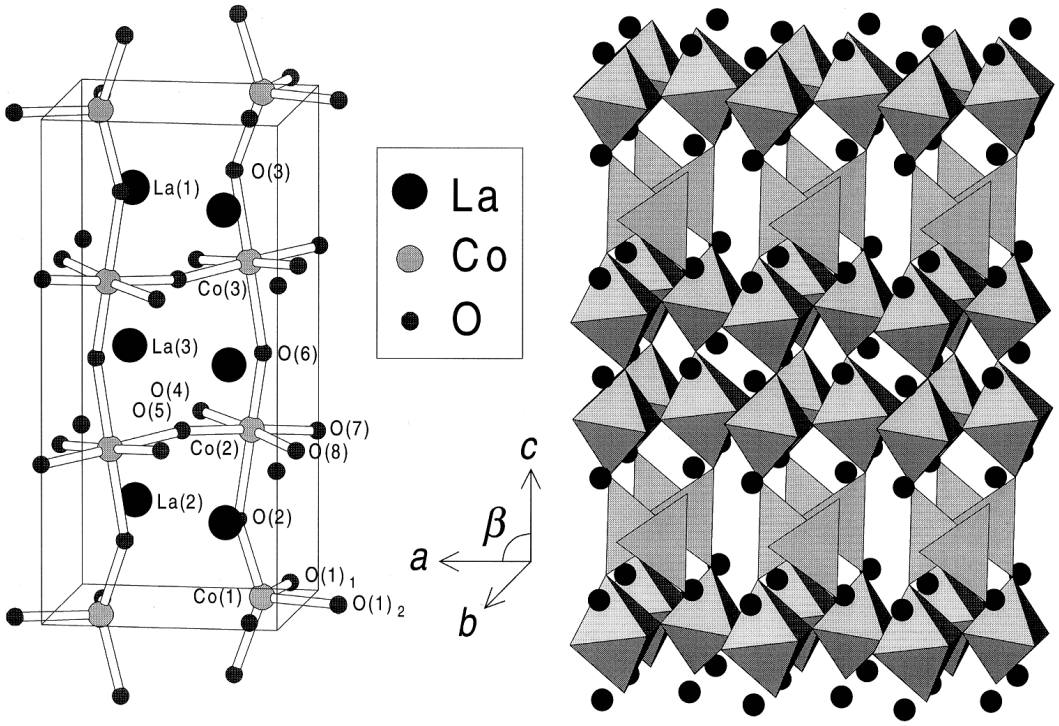

Fig. 7 Crystal structure for $La_3Co_3O_8$. Space group $P2_1$.

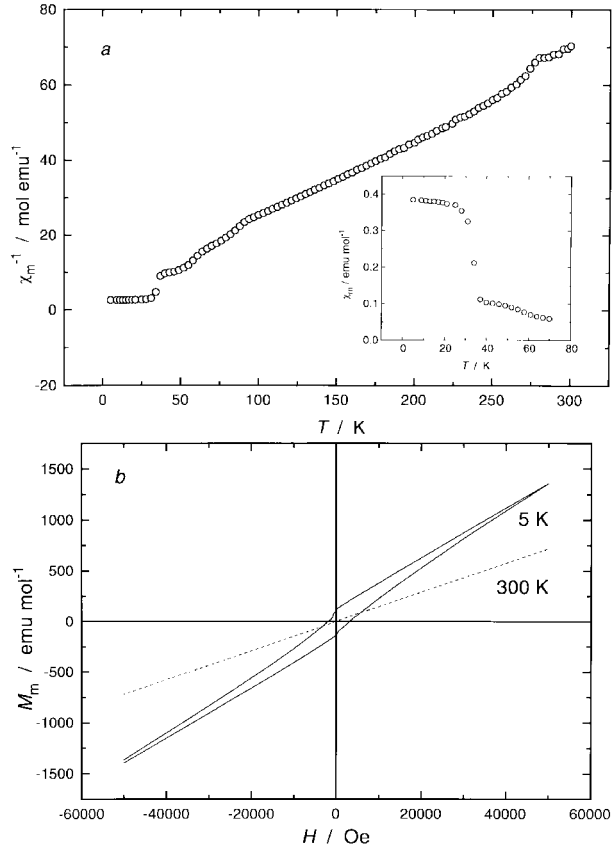

Fig. 8 (*a*) Temperature dependence of the inverse molar magnetic susceptibility (χ_m^{-1}) for $La_3Co_3O_8$, measuring field $H=200$ Oe. Inset shows the susceptibility (χ_m) at low temperatures. (*b*) Field dependence of the molar magnetisation for $La_3Co_3O_8$ at 5 K (—) and 300 K (---).

bility for $La_3Co_3O_8$ shows Curie–Weiss paramagnetic behaviour for temperatures above 35 K with paramagnetic moment per formula unit $\mu_p=5.9$ μ_B and Weiss constant $\Theta=-6$ K. The field (H) dependence of the magnetisation, Fig. 8(*b*), shows notably hysteresis at 5 K, whereas at 300 K the magnetisation shows no hysteresis. This could possibly indicate the coexistence of a weak ferromagnetic component at low temperatures. (Another possibility is the existence of a few microscopic particles of Co, of a few nm size, which are formed on the particle surfaces during the reduction.)

Long range magnetic ordering is confirmed by PND showing a number of additional reflections for temperatures below 35 K, Fig. 9 and 10. $LaCoO_3$, the pure Co^{III} member of the $La_nCo_nO_{3n-1}$ series ($n=\infty$) with Co^{III} in octahedral coordination, does not show long range magnetic order,[22] and Co^{III} is predominantly in the low-spin (LS) state at the lowest temperatures. For $La_2Co_2O_5$, the pure Co^{II} member of the $La_nCo_nO_{3n-1}$ series ($n=2$) with Co^{II} in both tetrahedral and octahedral coordination, all divalent cobalt atoms are in the high-spin (HS) state and antiferromagnetic order occurs below $T_N=301$ K.[3] It is hence reasonable to assume that octahedrally coordinated Co^{III} in $La_3Co_3O_8$ is in a diamagnetic low spin state for temperatures below T_N, whereas divalent, high-spin cobalt atoms carry a large antiferromagnetic moment. This is consistent with the low transition temperature which indicates

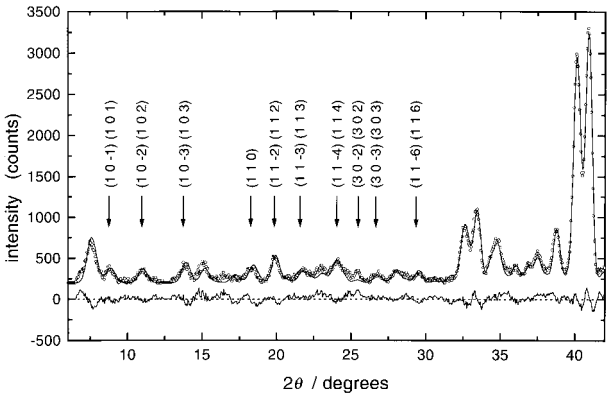

Fig. 9 Selected parts of the PND profile for $La_3Co_3O_8$ at 10 K ($\lambda=$ 153.79 pm) with emphasis on magnetic reflections marked with arrows and Miller indices are given. Experimental points marked by open circles, full line marks calculated profile, lower full line marks difference plot.

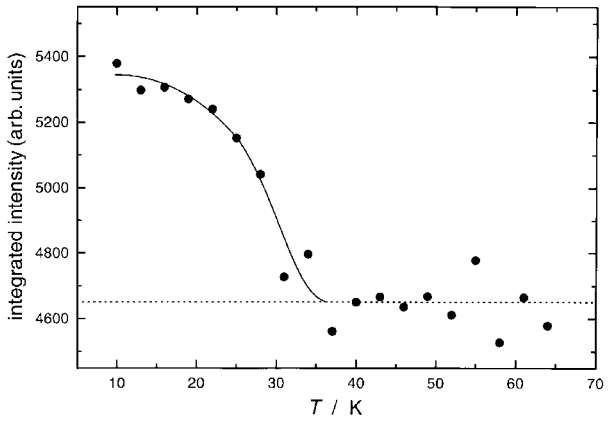

Fig. 10 Temperature dependence of the integrated intensity for the magnetic reflections (112) and (11$\bar{2}$). Dashed line represents the background level. Fully drawn line as guide to the eye.

an overall weak (antiferro)magnetic coupling. If Co^{III} were in a high-spin state, one would expect a strong antiferromagnetic coupling and high transition temperatures, in accordance with observations for the related phases $La_2Co^{II,HS}{}_2O_5$,[3] $La_4Co^{II,HS}{}_3O_9$,[23] and $Sr_2Co^{III,HS}{}_2O_5$.[24]

The magnetic reflections could be indexed on a magnetic unit cell (see Table 2) $\bar{a}_{mag}=2\bar{a}$, $\bar{b}_{mag}=\bar{b}$, and $\bar{c}_{mag}=2\bar{c}$. Within each chain of tetrahedrally coordinated Co^{II}, all cobalt atoms were assumed antiferromagnetically oriented relative to the two nearest neighbouring cobalt atoms for all tested models, *i.e.* similarly to that in $La_2Co_2O_5$ and $La_4Co_3O_9$. Initially, a large number of possible models for the magnetic structure were tested. Charge ordering for cobalt was first assumed as suggested by the bond valence calculations, with Co^{II}(HS) at the tetrahedral sites and half of the octahedral sites and with diamagnetic Co^{III}(LS) at the other half of the octahedral sites. The best results were obtained for a model with Co^{III}(LS) for Co(2) and Co^{II}(HS) for Co(1) and Co(3). The magnetic *R*-value was $R_M=23.1\%$. (The refined magnetic moments for Co^{II} were $\mu_{Co(1),\,tetr}=3.5\pm0.1\ \mu_B$ and $\mu_{Co(3),\,oct}=3.1\pm0.1\ \mu_B$.) However, the fit was improved by refining the magnetic moments (μ) for all the three different cobalt sites, hence allowing charge disorder at the two octahedral sites. The best fit was obtained when the [001]-components of the magnetic moments were fixed to zero, $R_M=19.1\%$. The results are given in Table 5 and Fig. 9. The proposed magnetic structure shown in Fig. 11 is rather complex with all the three different cobalt atoms (sites) having different magnitude and direction for their magnetic moments. The approximately equal and low values of the magnetic moment for Co(2) and Co(3) suggest a random distribution of Co^{II}(HS, $S=3/2$) and Co^{III}(LS, $S=0$) over these two sites. The direction and value of the magnetic moment for Co(1) is independent of the choice of starting values, whereas for the octahedrally coordinated cobalt atoms, Co(2) and Co(3), the directions are not precisely determined. For this reason the present magnetic structure must still be considered as approximate, as also indicated by the relatively high R_M-value and minor discrepancies between the observed and calculated intensity (Fig. 9). The values for the (total) magnetic moments of the octahedrally and tetrahedrally coordinated divalent cobalt atoms for $La_3Co_3O_8$ are slightly higher than

Table 5 Refined magnetic moments (in μ_B) for $La_3Co_3O_8$, see text; calculated standard deviations in parentheses

	$\mu_{[100]}$	$\mu_{[010]}$	μ
Co(1), tetrahedral	3.1(1)	−1.6(2)	3.5(1)
Co(2), octahedral	1.0(2)	−1.4(3)	1.7(2)
Co(3), octahedral	0.2(3)	2.0(2)	2.0(2)

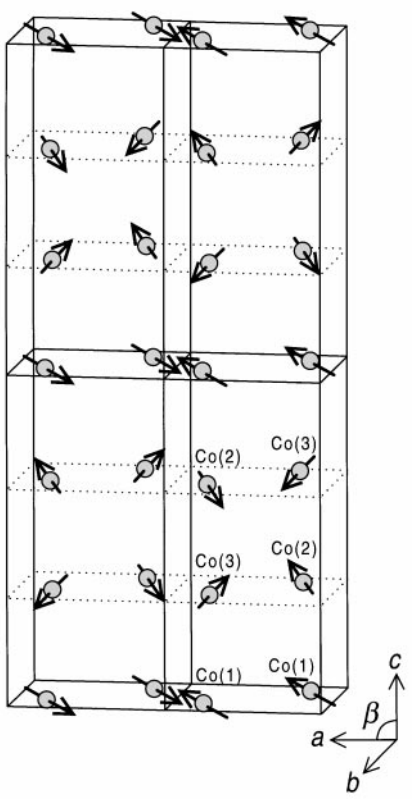

Fig. 11 Antiferromagnetic order in $La_3Co_3O_8$. Only Co atoms shown.

Table 6 Magnetic ordering temperatures (T_N) for phases in the La–Co–O system

	Co^{II}-fraction	T_N/K	ref.
$LaCoO_3$	0	—	22
$La_4Co_3O_{10}$	1/3	13	9
$La_3Co_3O_8$	2/3	35	this work
La_2CoO_4	1	275	25
$La_2Co_2O_5$	1	301	3
$La_4Co_3O_9$	1	303	23

the corresponding antiferromagnetic moments of Co^{II}(HS) for $La_2Co_2O_5$ and $La_4Co_3O_9$ [$\mu_{(Co^{II},\,tet)}=2.5\mu_B$ and $\mu_{(Co^{II},\,oct)}=3.0\mu_B$].[3,23]

The antiferromagnetic ordering temperatures for the different phases in the La–Co–O system, which are listed in Table 6 for comparison, shows that strong antiferromagnetic coupling between the cobalt atoms for these phases is closely connected to a high content of divalent cobalt.

This work has received financial support from the Research Council of Norway. Skilful assistance from the project team at the Swiss–Norwegian Beam Line, ESRF is gratefully acknowledged. Contribution No 98.4 from the Swiss–Norwegian Beam Line at ESRF.

References

1 M. Seppänen, M. Kytö and P. Taskinen, *Scand. J. Metall.*, 1979, **8**, 199.
2 K. Vidyasagar, A. Reller, J. Gopalakrishnan and C. N. R. Rao, *J. Chem. Soc., Chem. Commun.*, 1985, 7.
3 O. H. Hansteen, H. Fjellvåg and B. C. Hauback, *J. Solid State Chem.*, in press.
4 B. Gilbu Tilset, H. Fjellvåg and A. Kjekshus, *J. Solid State Chem.*, 1995, **119**, 271.
5 C. N. R. Rao, J. Gopalakrishnan and K. Vidyasagar, *Indian J. Chem. Sect. A*, 1984, **23**, 265.

6 M. J. Sayagués, M. Vallet-Regi, A. Caneiro and J. M. González-Calbet, *J. Solid State Chem*., 1994, **110**, 295.
7 J. C. Grenier, J. Darriet, M. Pouchard and P. Hagenmuller, *Mater. Res. Bull*. 1976, **11**, 1219.
8 A. Reller, D. A. Jefferson, J. M. Thomas and M. K. Uppal, *J. Phys. Chem*., 1983, **87**, 913.
9 O. H. Hansteen and H. Fjellvåg, *J. Solid State Chem*., in press.
10 B. Gilbu, H. Fjellvåg and A. Kjekshus, *Acta Chem. Scand*., 1994, **48,** 37.
11 P. E. Werner, L. Eriksson and M. Westdahl, Program TREOR (version 5), *J. Appl. Crystallogr*., 1985, **18**, 367.
12 Bengt Noläng, Program UNITCELL , Department of Chemistry, Uppsala University, Sweden.
13 A. C. Larson and R. B. Von Dreele, Program GSAS, General Structure Analysis System, LANSCE, MS-H 805, Los Alamos National Laboratory, Los Alamos, NM 87545, USA.
14 A. W. Hewat, Harwell Report RRL 73/239, 1973.
15 H. M. Rietveld, *J. Appl. Crystallogr*., 1969, **2**, 65.
16 J. Spreadborough and J. W. Christian, *J. Sci. Instrum*., 1959, **36,** 116.
17 M. A. Señarís-Rodríguez and J. B. Goodenough, *J. Solid State Chem*., 1995, **116,** 224.
18 K. R. Kendall, C. Navas, J. K. Thomas and H. C. zur Loye, *Solid State Ionics*, 1995, **82**, 215.
19 K. Yvon, W. Jeitschko and E. Parthe, *J. Appl. Crystallogr*., 1977, **10**, 73.
20 N. Nguyen, Y. Calage, F. Varret, G. Ferey, V. Caignaert, M. Hervieu and B. Raveau, *J. Solid State Chem*., 1984, **53**, 398.
21 I. D. Brown and D. Altermatt, *Acta Crystallogr*., *Sect. B*, 1985, **41**, 244.
22 G. Thornton, B. C. Toefield and A. H. Hewat, *J. Solid State Chem*., 1986, **61**, 301.
23 O. H. Hansteen, H. Fjellvåg and B. C. Hauback, *J. Mater. Chem*., 1998, **8**, following paper.
24 T. Takeda, Y. Yamaguchi and H. Watanabe, *J. Phys. Soc. Jpn*., 1972, **33**, 970.
25 K. Yamada, M. Matsuda, Y. Endoh, B. Keimer, R. J. Birgeneau, S. Onodera, J. Mizusaki, T. Matsuura and G. Shirane, *Phys. Rev. B*, 1989, **39,** 2336.

Paper 8/01796D; *Received* 4*th March*, 1998